Journal of Inflammation Research

Dovepress
open access to scientific and medical research

Open Access Full Text Article

ORIGINAL RESEARCH

Downregulation of Circular RNA Gla Reduced Astrocyte Inflammatory Status by Regulating miR-488/MEKK1 Levels and Promoted Functional Recovery After Spinal Cord Injury

Qiang Shao[1,2,*], Ying Zhang[2,*], Zhiyuan Zhang[2], Wei Jiang[2], Yongcheng Yin[3], Yuepeng Fang[1], Ce Zhang[1], Qingfa Chen[2], Bin Ning[1,2]

[1]Cheeloo College of Medicine, Jinan Central Hospital, Shandong University, Jinan, People's Republic of China; [2]Central Hospital Affiliated to Shandong First Medical University, Shandong First Medical University & Shandong Academy of Medical Sciences, Jinan, Shandong, People's Republic of China; [3]School of Clinical Medicine, Shandong Second Medical University, Weifang, People's Republic of China

*These authors contributed equally to this work

Correspondence: Bin Ning; Qingfa Chen, Central Hospital Affiliated to Shandong First Medical University, No. 105, Jiefang Road, Jinan, Shandong, 250013, People's Republic of China, Tel +86-18866510349, Email bning@sdfmu.edu.cn; tsingfachan@163.com

Background: Post-spinal cord injury (SCI) inflammation correlates with neurologic recovery. Through sequencing, we explored the roles of a differentially expressed circRNA in mice after SCI, circGla, on inflammation and recovery of SCI.

Methods: The T8–T10 SCI model was established in C57BL6 mice. HE staining and RT-qPCR verified circGla upregulation results after injury obtained through sequencing. RNase R digestion and primer amplification experiments confirmed the circular properties of circGla. Nucleus and cytoplasm isolation experiments and FISH confirmed circGla expression in the astrocyte cytoplasm. AAV was used to establish a circGla knockdown mouse model. Behavioral tests were conducted to assess the recovery of the neurological function. The key inflammatory molecules after SCI were evaluated through MRI, RT-qPCR, and ELISA. For in vitro experiments, circGla was upregulated or knocked down in mouse astrocytes to detect its effect. The binding between miR-488 and circGla was confirmed through RIP and the dual luciferase experiment. RT-qPCR and ELISA confirmed the content correlation of the two molecules and the in vitro inflammatory function of miR-488. The binding experiment in astrocytes confirmed the binding between miR-488 and MEKK1 mRNA. Western blotting of MAPK pathway-related proteins confirmed that MEKK1 is a downstream effector for circGla and miR-488 in astrocytes.

Results: Following SCI, the circular RNA circGla levels increased and it existed in the astrocyte cytoplasm. circGla knockdown reduced inflammation and improved neurological recovery in vivo. The correlation between circGla and proinflammatory factors was confirmed in vitro. circGla bound to miR-488, and the high miR-488 level was associated with the low astrocyte inflammatory state. miR-488 bound to MEKK1 mRNA, and upregulation or knockdown of circGla or miR-488 affected MAPK pathway-related protein expression.

Conclusion: Following SCI, downregulation of circGla expression in astrocytes can reduce inflammatory manifestations and stimulate long-term functional recovery in mice through miR-488 and MEKK1.

Keywords: non-coding RNAs, inflammation, competing endogenous RNAs, traumatic spinal cord injury, secondary injury

Introduction

Spinal cord injury (SCI) is a very serious class of traumatic diseases affecting the central nervous system (CNS) and is among the most severe public health problems worldwide.[1–3] Traumatic SCIs comprise a vast majority of SCI etiologies. SCI causes severe long-term neurological damage in a patient, and the number of SCI cases is increasing. Thus, SCI is a severe societal hazard and results in a loss of global human potential.[4,5] Effective treatments for coping with the enormous challenge of nerve

Received: 8 March 2024
Accepted: 21 September 2024
Published: 9 October 2024

Graphical Abstract

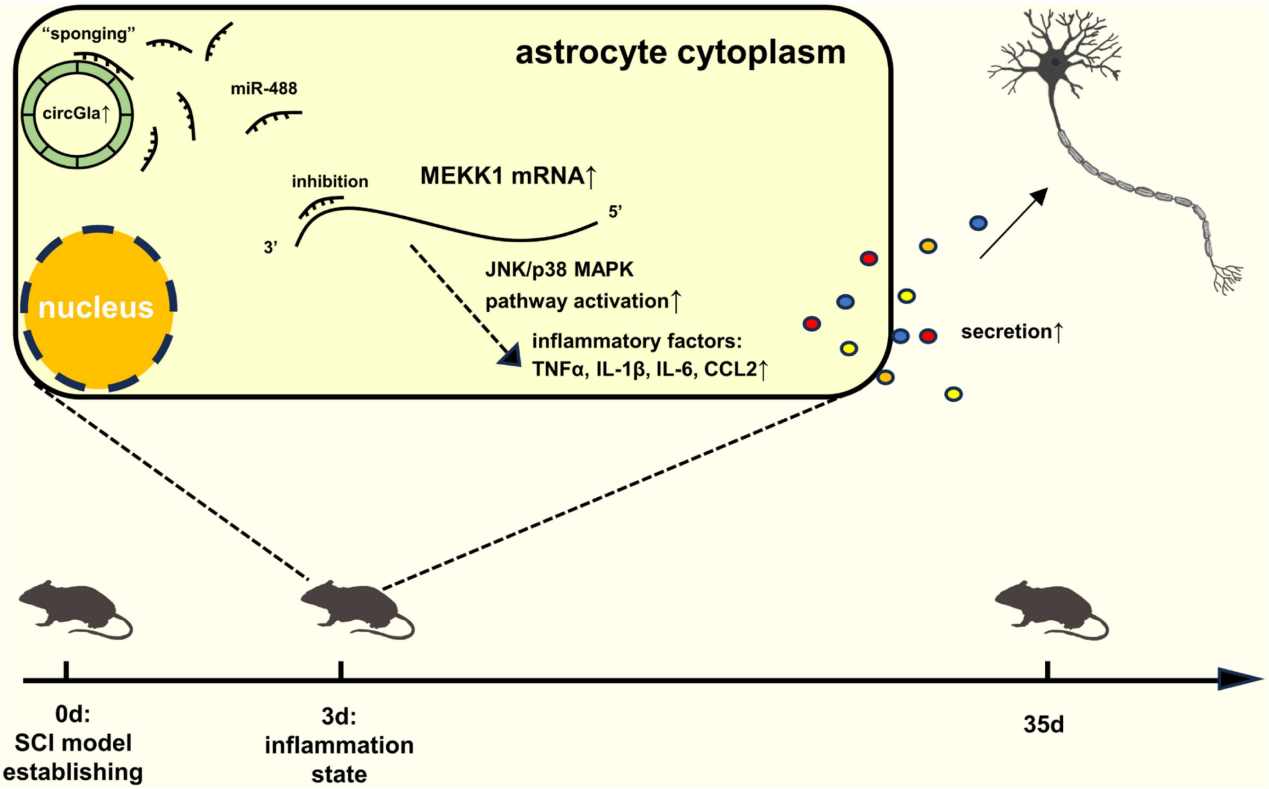

regeneration and neurological reconstruction after SCI are lacking. In pathophysiology, the SCI process is categorized as the initial primary injury and the chronic secondary injury.[6,7]

Inflammation is a major event in the secondary injury, and the cascading and amplifying properties of inflammation lead to more neuronal damage. Inflammation is a crucial determinant of the extent and magnitude of injury, which profoundly affects SCI outcomes.[7,8] In a murine SCI model, the spinal cord continues to exhibit active inflammation 3 days post-SCI (dpi), with inflammatory factors (IL-1β, IL-6, TNF-α) still on the rise.[7] As the most numerous spinal cord-resident glial cells, astrocytes perform vital homeostatic maintenance functions.[9] Damaged cellular debris (damage-associated molecular patterns, DAMPs) and associated intracellular proteins released in the surrounding microenvironment cause heterogeneous activation of astrocytes from the resting stage, which then participate in inflammatory cascades.[10,11] The intervention on cellular components of early inflammation for influencing long-term neurological recovery is a potential therapeutic strategy.

Among the known non-coding RNAs, circular RNAs (circRNAs) have been extensively studied in various diseases (eg, cancers, cardiovascular diseases, and CNS diseases).[12–17]circRNAs primarily serve as sponges for microRNAs (miRNAs) and RNA-binding proteins, thereby leading to post-transcriptional regulation and alteration of cellular phenotypes.[18,19] The role of circRNAs in CNS disorders, including SCI, has been documented.[16] However, a more definitive and in-depth exploration of the role of circRNAs in the post-SCI inflammatory process is required. Additionally, further studies are warranted for elucidating circRNA differential expression before and after SCI.

Our group analyzed changes in circRNA contents in the SCI mouse model. The significantly differentially expressed circRNA at 3 dpi, namely circGla, was selected to explore its role and mechanism in inflammation and neurological function recovery in SCI. Our study investigated the molecular binding and functional interactions of circGla and its downstream molecules, miR-488 and MEKK1, in astrocytes after SCI. The aforementioned three molecules affected the inflammatory

state of the spinal cord and neurological recovery after SCI. circGla can potentially be used as a marker and a target for future SCI treatment.

Material and Methods

Adeno-Associated Virus Injection and SCI Modeling

Female C57BL6 mice (age: 5 weeks, weight: 16–18 g) were purchased from Beijing Vital River Laboratory Animal Technology Co., Ltd (Beijing, China). The mice were housed in a 12-h light–dark alternating, 22°C ± 2°C constant temperature SPF animal room in Jinan Central Hospital. The mice had free access to food and water. For the experiments conducted to assess the inflammatory states and motion function recovery, the animals were randomized into the following groups: sham group, sham+sh-NC group, SCI+sh-NC group, and SCI+sh-circGla group with SCI. Adeno-associated viruses (AAVs) (sh-NC AAV: pAAV-U6-shNC-CMV-EGFP-WPRE; sh-circGla AAV: pAAV-U6-shcircGla-CMV-EGFP) were constructed by Obio Technology (Obio, Shanghai, China). After all the mice were acclimatized to the feeding environment, they were intrathecally injected with sh-NC AAV or sh-circGla AAV or not. After 4 weeks, the virus reached its maximum effect. The SCI group mice anesthetized with 3% pentobarbital, underwent dorsal dermatotomy and T8–T10 laminectomy, and received a standard SCI impact (impact depth: 2 mm; impact velocity: 1 m/s; residence time: 1 s), which was applied using a precision pneumatic spinal cord impactor (RWD Life Science, 68100, Shenzhen, China), and underwent suture surgery. The sham group mice received the same procedure as the SCI group mice, except for the impact process. After the animals regained consciousness, they were placed back in the cage, and the bladder was squeezed daily until the mice started urinating. The sh-circGla AAV sequence is provided in Supplemental Table 1. The animal experiments were approved by the Welfare and Ethics of Experimental Animals Committee, Jinan Central Hospital (approval No. JNCHIACUC-202114; guideline: National Standard of the People's Republic of China GB/T 35892–2018 Guidelines for Ethical Review of Laboratory Animal Welfare).

Tissue and Serum Preparation

On the 28th day after AAV injection, the mice underwent the sham or SCI modeling procedure. At 3 dpi, the mice were anesthetized with 3% pentobarbital (30 mg/kg, Sigma) for subsequently detecting the AAV transfection efficacy and testing inflammatory states. After the transcardiac blood was sampled for the enzyme-linked immunosorbent assay (ELISA) and cardiac perfusion, 1 cm-long spinal cord tissues were removed symmetrically from above and below the central point of SCI. The tissues were preserved in cryopreservation tubes, and the tubes were immediately stored in liquid nitrogen. Some tissues were washed in PBS (Solarbio, Beijing, China) and used for RT-qPCR. The remaining tissues were soaked in a 4% paraformaldehyde solution (Biosharp, Hefei, China). Then, xylene and alcohol solutions in a gradient were used for dehydration. The tissues were embedded in paraffin wax and cut into 5-μm continuous sections for the subsequent immunofluorescence experiments. The blood prepared for ELISA was centrifuged (3500 rpm, 15 min) to collect the serum, which was preserved at −80°C.

Behavioral Scoring

The Basso Mouse Scale (BMS) scores of the mice were determined at critical time points (0, 1, 3, 7, 14, 21, 28, and 35 dpi). Based on the previously reported BMS scale,[20] we assessed and scored the mice on a 0–9 scale for behavior, with a better motor function being associated with higher scores.

For the inclined plane test conducted at 0, 1, 3, 7, 14, 21, 28, and 35 dpi, the mice were placed on a rough inclined plane. The longitudinal axis of the mouse body was placed parallel to the inclined axis of the plane, with the head directed to the uplifted side. Then, the inclined plane was tilted incrementally from zero. We then recorded the maximum inclined angle at which the mice remained stable in the plane for 5 s without dropping off. The average of three repetitions of the test was used as the recorded value for each mouse. Experienced and blinded experimenters conducted both BMS scoring and the inclined plane test.

Open Field Test

At 28 dpi, the mice were subjected to open-field experiments to assess motor function recovery. A 45*45*35 (L*W*H) open field equipped with an infrared detection system (Saeons Company, Saeons, China) recorded the position and trajectory of the mouse movement in the field. The total distance moved by the mice in 5 min was also recorded. Before the start of the experiment, each mouse was acclimatized to the open field environment, and its bladder was emptied. At the beginning of the experiment, the mice were placed in the same corner of the experimental setup and allowed to move freely for 5 min.

Animal Magnetic Resonance Imaging

At 3 dpi, the mice in the two SCI groups were subjected to magnetic resonance imaging (MRI) by using a 9.4T small animal MRI scanner instrument (Bruker Biospec, Germany) after being anesthetized with 1.5% isoflurane (RWD Life Science, Shenzhen, China). T2-weighted sagittal images were acquired using the Bruker ParaVision 6.0 system.

Acquisition and Culture of Primary Mouse Astrocytes and C8D1A Mouse Astrocytes

Primary mouse astrocytes were purchased from ScienCell Research Laboratories (San Diego, CA, USA). C8D1A mouse astrocytes were purchased from Zhong Qiao Xin Zhou Biotechnology (ZQXZ Biotechnology, Shanghai, China). All cells were cultured in Dulbecco's Modified Eagle Medium (Gibco, CA, USA) supplemented with 1% penicillin-streptomycin and 10% fetal bovine serum (Gibco) at 37°C with 5% CO_2. Mouse TNF-α (MCE, USA) was used to stimulate astrocytes for an inflammatory condition.

siRNA, Overexpression Plasmid, and miRNA Inhibitors and Mimics

RiboBio company (RiboBio, Guangzhou, China) designed and synthesized the circGla siRNA (target sequence: ACCCTTTCATAAGTGAGCA), and miR-488 mimics and inhibitors. The overexpression plasmid for circGla was constructed by Obio Technology.

The C8D1A mouse astrocytes were passage into 6-well plates. To study circGla downregulation and upregulation, the corresponding siRNA or overexpression plasmid was transfected using the riboFECT CP Transfection Kit (RiboBio) or Lipofectamine 2000 (Thermo Fisher Scientific, CA, USA), respectively, according to the manufacturer's instructions. To analyze miR-488 downregulation and upregulation, miR-488 inhibitors or mimics were transfected using the riboFECT CP Transfection Kit. Then, 10 ng/mL TNF-α was added to the culture medium and incubated for 24 h after transfection. Another 24 h later, the supernatant and cells were collected for ELISA or RT-qPCR.

Real-Time Quantitative Polymerase Chain Reaction (RT-qPCR)

Using the AG RNAex Pro Reagent (Accurate Biology, Changsha, China), RNA was extracted from the spinal cord tissues and cells. circRNA, miRNA, and mRNA reverse transcription reactions were carried out using the Evo MMLV Reverse Transcription Kit (Accurate Biology, Changsha, China). The temperature was adjusted on a T100™ Thermal Cycler (Bio-Rad, Hercules, CA, USA). The Premix Pro Taq HS qPCR Kit (Accurate Biology, Changsha, China) was used for establishing the amplification system. LightCycler480 II (Roche, Indianapolis, IN, USA) was used for complementary DNA amplification. DNA expressions were normalized using the internal reference, and the relative expression was calculated using the $2^{-\Delta\Delta CT}$ method. Supplemental Table 1 lists all primer information.

Dual-Luciferase Reporter Assays

Mouse astrocyte C8D1A was used to bind circGla with miR-488 or miR-488 with MEKK1 mRNA. Briefly, vector construction was achieved by using pmirGLO or pGL3-Basic plasmids (BioSune, Jinan, China) with circGla or the MEKK1 mRNA 3′-UTR (WT: ACAGGCCGAAGCAUUGUAUACUCCUGUGAGUGGCCACUUUAUUUGAG ACCCUUUCAUAAG; MUT: ACAGGCCGAAGCAUUGUAUACUCCUGUGAGUGGCCACUUUAUUUGAGACUUC CCUGUAAG). The mutant plasmids were synthesized similarly. Thereafter, C8D1A cells were transfected with plasmids with the wild-type (WT) or mutant (MUT) sequence and miR-488 mimics or mimics NC (RiboBio) for 2 days. The expression

intensity of fluorescence was measured by using the Promega Dual-Luciferase Reporter Assay System (Promega, Madison, WI, USA) according to the manufacturer's instructions.

RNA Immunoprecipitation

RNA immunoprecipitation (RIP) assays were performed using the Magna RIP RNA-Binding Protein Immunoprecipitation Kit (Millipore, Bedford, MA, USA). According to the instructions, the astrocytes were lysed using RIP lysis buffer. The cell lysates were incubated with magnetic beads containing the anti-argonaute-2 (AGO2) antibody (Millipore, Billerica, MA, USA) or rabbit anti-IgG antibody (Millipore, Billerica, USA). Finally, RNA was extracted and detected using Trizol and through RT-qPCR.

Hematoxylin–Eosin Staining

The spinal cord tissue was stained using a hematoxylin–eosin (HE) staining kit (Servicebio, Wuhan, China) according to the manufacturer's instructions. The paraffin-embedded spinal cord was placed in a baking oven at 60°C for 1 h and cut into sections. The slices were then placed in xylene and alcohol solutions in a gradient. The paraffin sections were stained with hematoxylin solution for 3 min, washed with tap water, treated with the hematoxylin differentiation solution, and rinsed with tap water. Thereafter, the sections were treated with the hematoxylin Scott Tap Bluing Reagent and rinsed with running water. The paraffin sections were dehydrated separately with 85% and 95% alcohol solutions, stained with eosin solution for 5 min, dehydrated with xylene and graded alcohol solutions, and sealed with neutral gum. The sections were observed and photographed using a microscope (Olympus, Tokyo, Japan).

Immunofluorescence Staining

For spinal cord staining, the paraffin sections were first dewaxed using xylene and graded alcohol solutions. Antigen repair was performed using a boiled citrate solution (pH = 6). The sections were blocked with the normal goat serum and co-incubated with the following primary antibodies: mouse anti-GFAP (CST, 3670s, 1:500) and rabbit anti-GFP (GFP, Cloud clone PAD025Ge07, 1:100) at 4°C overnight. The next day, the tissues were incubated with the following secondary antibodies: goat anti-mouse IgG H&L (Abcam, Alexa Fluor® 594, ab150116, 1:200) and goat anti-rabbit IgG H&L (Abcam, Alexa Fluor® 488, ab150077, 1:200) for 1 h at 37°C. Cell nuclei were stained using DAPI. The images are observed and photographed using an electron microscope (Olympus).

Enzyme-Linked Immunosorbent Assay

The astrocytes were grown in 6-well plates. After the siRNA or overexpression plasmid was transfected and TNF-α was added to induce inflammation, the medium supernatant was collected. Using the serum or supernatant, ELISA was conducted for IL-1β, IL-6, and CCL2 according to the manufacturer's instructions (Invitrogen, Shanghai, China). Absorbance was measured using the enzyme marker (Molecular Devices, Shanghai, China).

Fluorescence in situ Hybridization Assay

The RiboBio in situ hybridization kit (RiboBio) was used to detect circGla expression in the primary astrocytes. RiboBio synthesized the probe for circGla. The astrocytes were fixed using 4% paraformaldehyde, permeabilized using 0.1% Triton X-100, incubated with a pre-hybridization solution at 37°C for 30 min, and incubated with the circGla probe-containing hybridization solution. The next day, the nuclei were stained with DAPI.

Sanger Sequencing

After 20 min of treatment with RNase R at 37°C, circRNAs were purified from the total RNA. To probe the circGla junction sequence, we performed Sanger sequencing according to the manufacturer's instructions (Thermo Fisher Scientific, Shanghai, China).

Agarose Gel Electrophoresis

To obtain the 1.2% agarose gel, the agarose powder (Yeasen, Shanghai, China) was completely dissolved in 1×Tris acetate-EDTA buffer (Solabio) with heating. The dissolved powder was mixed and allowed to cool to 60°C. The 10000× nucleic acid gel stain (Yeasen) was added to the dissolved powder and mixed. The liquid was poured into the glue mold in which a comb was inserted and allowed to solidify. The comb was removed, and the gel block was transferred to the electrophoresis tank. Then, the sampling buffer containing circGla or Gla divergent or convergent primer PCR amplification products and DNA dye of the same volume were added to each lane. The voltage was set at 120 V, and electrophoresis lasted 40 min with a Bio-Rad power supply (Bio-Rad, USA). Subsequently, the gel block was placed under a gel imager (FluorChem M, Proteinsimple). Supplemental Table 1 presents the sequences of the divergent and convergent primers.

Nuclear and Cytoplasmic Separation and Extraction

Primary mouse astrocytes were washed with PBS and centrifuged to collect the nuclear and cytoplasmic content. We then used the PARISTM Kit for extracting RNA (Invitrogen, Shanghai, China) according to the manufacturer's protocols. RNA from the nucleus and plasma was separately collected for RT-qPCR.

Western Blotting

Proteins were extracted from the mouse astrocytes and separated through 10% SDS-PAGE. Then, the proteins were transferred to a nitrocellulose membrane. Tris-buffered saline with 0.1% Tween-20 and 5% skimmed milk was used to block the nitrocellulose membrane for 2 h at room temperature. The membrane was washed and incubated with primary antibodies and horseradish peroxidase (HRP) labeled secondary antibodies. Antibodies and their dilution ratios are listed in the next subsection. The membrane was visualized using the ECL detection reagent (Yeasen) and a gel imager (FluorChem M, Proteinsimple). The blot images were quantified using ImageJ software.

Antibodies for Western Blotting

MEKK1 polyclonal antibody (1:1000, 19,970-1-AP, Proteintech, Wuhan, China), p38 MAPK polyclonal antibody (1:2000, 14,064-1-AP, Proteintech), phospho-p38 MAPK polyclonal antibody (1:1000, 28,796-1-AP, Proteintech), JNK monoclonal antibody (1:3000, 66,210-1-Ig, Proteintech), phospho-JNK recombinant antibody (1:1000, 80,024-1-RR, Proteintech), GAPDH mouse monoclonal antibody (1:10000, AC033, Abclonal, Wuhan, China), Vinculin polyclonal antibody (1:10,000, 26,520-1-AP, Proteintech), HRP-conjugated goat anti-rabbit IgG (H+L) (1:2000, AS014, Abclonal), and HRP-conjugated goat anti-mouse IgG (H+L) (1:2000, AS003, Abclonal) were used.

Statistical Analysis

Statistical analysis was performed using GraphPad Prism software (version 8.0.1 for Windows, GraphPad Software, San Diego, California USA, www.graphpad.com). Student's *t*-test was conducted to compare differences between the two groups. One-way analysis of variance was applied to compare differences between three or more groups. Data are expressed as mean ± standard deviation. Differences are considered significant at $P < 0.05$.

Results

circGla Was Upregulated After SCI and Located in the Astrocyte Cytoplasm

Through our previous circRNA-sequencing containing 3 dpi examples of 3 SCI and 3 sham surgery mouse spinal cord tissues (Figure S1A and B), the circGla expression significantly increased after SCI. Using 5-week-old female C57BL6 mice, the SCI model was established with a precision pneumatic spinal cord impactor having an impact depth and impact velocity of 2 mm and 1 m/s, respectively. At 3 dpi, to examine the efficacy of our SCI model, 1-cm-long spinal cord tissues around the injury sites from the sham or SCI group mice were extracted and stained with HE. Compared with the spinal cord of the sham group mice, the spinal cord tissues in the injury group mice exhibited significant manifestations of swelling, infiltration of blood and inflammatory cells, and vacuole formation (Figure 1A), which indicated that SCI modeling was successful. To confirm the increase in circGla expressions observed in previous sequencing results, the

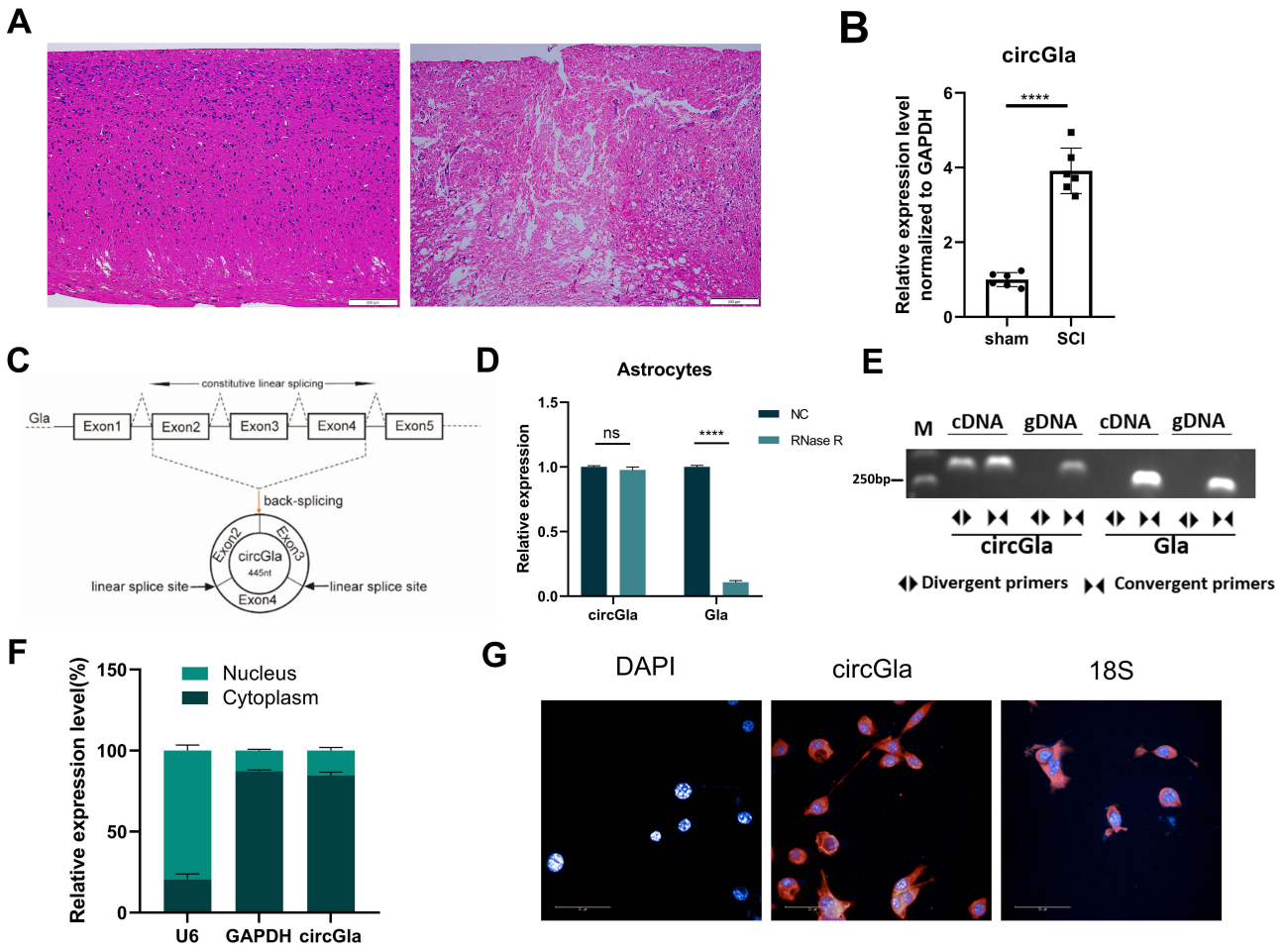

Figure 1 The content, circular characteristics, and astrocyte cytoplasmic location of circGla. (**A**) HE staining from mouse tissue sections under sham (left panel) and SCI 3d (right panel) conditions. Scale bar: 200 μm. (**B**) The relative expression folds of circGla relative to GAPDH in sham and SCI 3d mouse spinal cord. RT-qPCR results (n = 6). (**C**) Schematic diagram of the circGla-generation process. Transcription and back-splicing of parental gene Gla exons 2–4 generate circGla. (**D**) RNase R digestion experiment proved the circular characteristic of circGla. Mouse astrocyte lysis was treated without or with RNase, after which RT-qPCR was used to detect the mRNA levels of circGla. (**E**) The results of agarose gel electrophoresis revealed that circGla was amplified with divergent primers in cDNA, but not in gDNA. Gla was used as a linear gene control. (**F**) The relative mRNA expressions of circGla in the mouse astrocyte cytoplasm and nucleus were detected by RT-qPCR. GAPDH was used as a reference in the cytoplasm. U6 served as the nuclear control. (**G**) RNA FISH was used to confirm the cytoplasm location of circGla in mouse astrocytes. DAPI shows the nucleus. 18S rRNA was used as the cytoplasm control. Scale bar: 50 μm. ns: no significance; ****P < 0.0001.

total RNA of spinal cord tissues on 3 dpi was extracted and subjected to RT-qPCR (Figure 1B). The results indicated that circGla levels were upregulated to 4 times in the SCI tissue compared with the sham tissue, which is similar to the circGla results obtained in circRNA sequencing. Analysis of the circGla nucleotide sequence through Sanger sequencing further confirmed its head-to-tail circular structure (Figure 1C). To verify that circGla is indeed circular, the RNase R experiment was conducted, followed by RT-qPCR (Figure 1D). The RNase R treatment significantly decreased the linear mRNA levels of Gla, whereas circGla expressions remained relatively unchanged. Considering that head-to-tail splicing can also be a result of genomic rearrangement, we designed convergent and divergent PCR-specific primers of circGla and its parental gene Gla (serving as a control) to perform PCR by using the genomic DNA or cDNA from the primary mouse astrocytes as templates. Agarose gel electrophoresis revealed that circGla was only amplified by the divergent primers from the cDNA but not from the gDNA (Figure 1E), thereby ruling out the possibility of genome rearrangement. Next, the subcellular location of circGla in the mouse astrocytes was determined through RT-qPCR of nuclear and cytoplasmic extracts (Figure 1F) and the fluorescence in situ hybridization (FISH) assay with the circGla fluorescence probe (Figure 1G).

circGla Downregulation in the SCI Mouse Model Promoted Functional Recovery and Alleviated the Inflammatory State

Based on the validation of upregulated circGla expression in the spinal cord tissue at 3 dpi, we investigated whether this upregulation in circGla during the acute inflammatory phase is pivotal for short-term inflammatory manifestations and long-term functional recovery after SCI in vivo. GFP sequence-containing sh-AAV was used to downregulate circGla expressions in the mouse spinal cord. The transfection efficacy of GFP sequence-containing sh-AAV into mouse astrocytes was validated based on the co-location of GFAP (an astrocyte marker) and GFP in the immunofluorescence staining of spinal cord tissues 14 days after sh-AAV or sh-NC was intrathecally injected and RT-qPCR of RNA from the spinal cord tissues of the mice (Figure 2A and B). The 5-week-old C57BL6 female mice were randomized into four groups: mice not injected with AAV at −28 dpi and sham-operated at 0 dpi (sham group), mice intrathecally injected with sh-NC AAV at −28 dpi and sham-operated at 0 dpi (sham+sh-NC group), mice injected with sh-NC AAV at −28 dpi and receiving the T8−T10 spinal cord impact at 0 dpi (SCI+sh-NC group), and mice injected with sh-circGla AAV on −28 dpi and receiving the T8−T10 spinal cord impact on 0 dpi (SCI+sh-circGla group). At 0, 1, 3, 7, 14, 21, 28, and 35 dpi, the BMS scoring and the inclined plane test were conducted to assess the behavior recovery states of every group after SCI (Figure 2C). Compared with the SCI+sh-NC group, the SCI+sh-circGla group exhibited significant functional improvement in BMS scoring after 21 dpi (Figure 2D) and in the inclined plane test after 14 dpi (Figure 2E). At 28 dpi when the SCI group mice attained significant recovery, the open field test was conducted to detect functional recovery in the mice in each group. The sh-NC AAV injection caused no significant deterioration in the sham groups. By contrast, significant functional recovery was observed in the SCI+sh-circGla group compared with the SCI+sh-NC group. This was indicated by the representative images of the motion path (Figure 2F) and the quantified corresponding total motion distance charts (Figure 2G) for mice in each group. Given the considerable long-term functional improvement, we focused on determining the exact pivotal role of circGla in the inflammatory state at 3 dpi, the acute inflammatory phase of SCI. Representative small animal MR images displayed a relatively milder inflammation manifestation at the injury site in the SCI+sh-circGla group compared with the SCI+sh-NC group (Figure 2H). mRNA levels of the major inflammatory cytokines (TNF-α, IL-1β, and IL-6) in the spinal cord tissues of the mice in each group and their serum protein levels were detected through RT-qPCR and ELISA, respectively (Figure 2I–N). The sh-NC injection caused no apparent alternation in the mRNA and protein levels. By contrast, the sh-circGla AAV injection significantly upregulated the mRNA and protein levels of the aforementioned cytokines compared with the SCI+sh-NC injection. In summary, the aforementioned results indicated that circGla affected both the spinal cord's inflammatory state in the mice during the acute inflammatory phase and the long-term recovery of SCI.

circGla Knockdown or Overexpression Caused Changes in the Inflammatory Mediator in Astrocytes

The inflammatory state in the acute phase majorly affects the outcome of SCI.[21] While in vivo experiments confirmed the effect of circGla alternation on the acute inflammatory phase after SCI, its inflammation-related function had not been well illustrated in in vitro experiments. Considering the abundance of cytoplasmic circGla expression in the mouse astrocytes, the co-location of GFAP and GFP in IF staining, and the different transfection efficacies on cell lines and primary cells, the C8D1A mouse astrocyte was selected in the subsequent in vitro experiment. To mimic the post-SCI microenvironment in vitro, a series of TNF-α concentration and time gradients were established, and the treatment condition of 24 h and 10 ng/mL TNF-α, where circGla expressions were the highest, was selected for the next in vitro experiments (Figure 3A and B). To investigate the role of circGla in post-SCI inflammation, siRNA or plasmids were transfected into the mouse astrocytes to upregulate or downregulate circGla expression (Figure 3C and D). When circGla was downregulated, IL-1β, IL-6, and CCL2 levels decreased compared with those in the NC group (Figure 3E–G). By contrast, when circGla was upregulated, the mRNA levels exhibited an opposite trend compared with those in the NC group. Furthermore, ELISA was performed to analyze the expression of the proinflammatory cytokines IL-1β, IL-6, and CCL2 (Figure 3H–J) in the supernatant of each group transfected with the siRNA or plasmid. IL-1β, IL-6, and CCL2 expression increased in the OE group compared with the NC group, whereas it decreased in the knockdown group compared with the NC group.

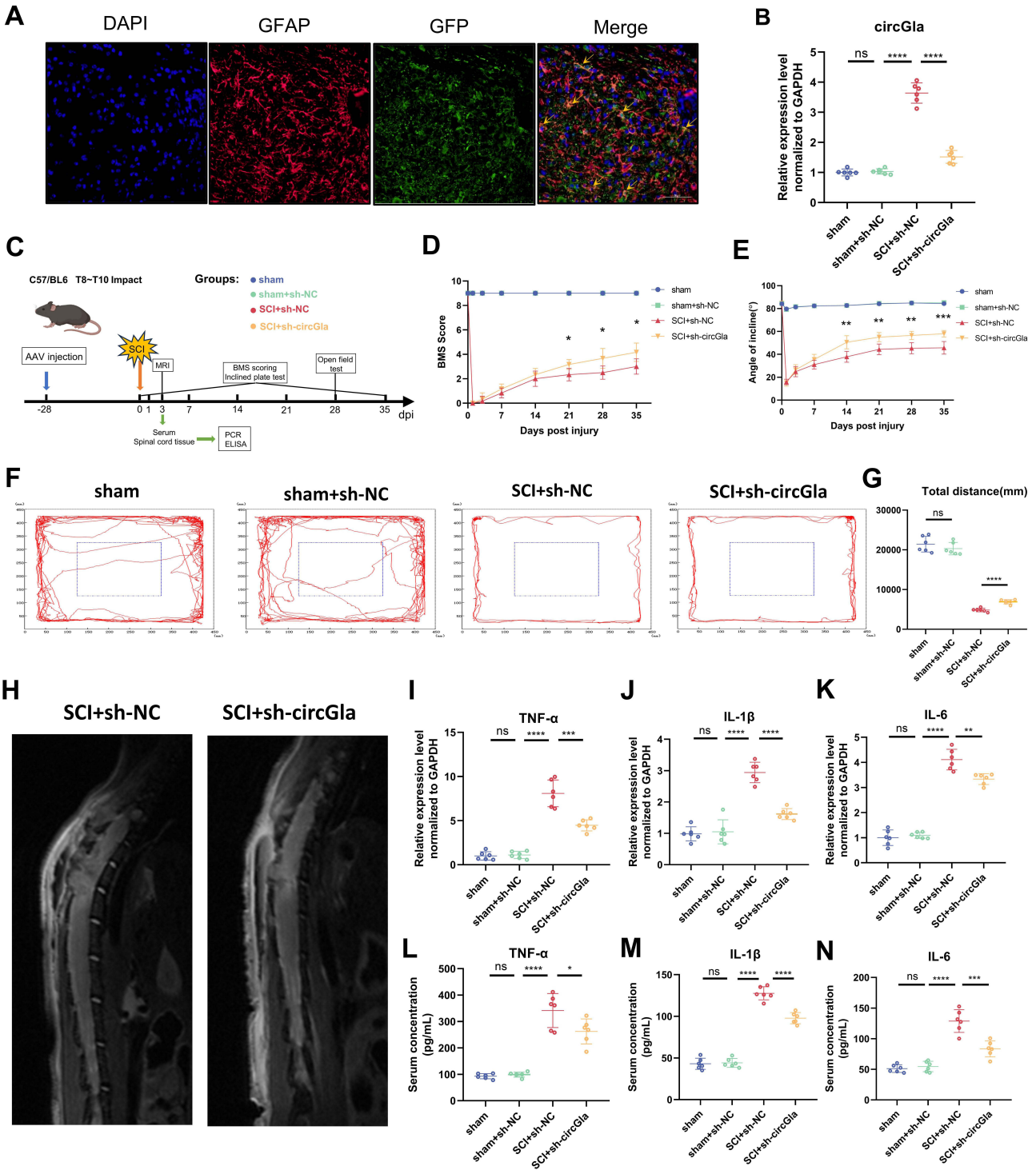

Figure 2 Effects of in vivocircGla downregulation on the functional recovery and inflammation. (**A**) GFAP and GFP co-location (yellow arrows) in mouse spinal cord immunofluorescence images indicated after intrathecal injection, and sh-circGla AAV successfully infected astrocytes in the spinal cord of C57BL6 mice. DAPI, blue; GFAP, red; GFP, green. Scale bar: 50 μm. (**B**) RT-qPCR of the circGla mRNA expressions in different groups (n = 6). Injection of sh-circGla AAV downregulated circGla. GAPDH served as an internal reference. (**C**) Sketch map of major animal experiments in this study. Created in BioRender. Shao, Q. (2024) BioRender.com/o77y647. (**D**) BMS scoring of 0–5 weeks after SCI in different groups (n = 6). (**E**) Angles of inclined plane test for mice 0–5 weeks after SCI in different groups were recorded (n = 6). (**F** and **G**) Representative images of open field test on 28 dpi for mice in different groups (**F**) and the summary quantitative image for the total distance (**G**) n = 6. (**H**) Representative animal MRI images in the T2 phase showed that the spinal cord of SCI 3d mice in the sh-circGla group contained milder inflammation manifestations. (**I–K**) RT-qPCR of the sham and SCI 3d mouse spinal cord tissues revealed the relative mRNA levels of key inflammatory mediators (ie, TNF-α, IL-1β, IL-6). n = 6. (**L-N**) ELISA for key inflammatory mediators (ie, TNF-α, IL-1β, IL-6) in the serum of the sham and SCI 3d mice. n = 6. ns: no significance; *P < 0.05; **P < 0.01; ***P < 0.001; ****P < 0.0001.

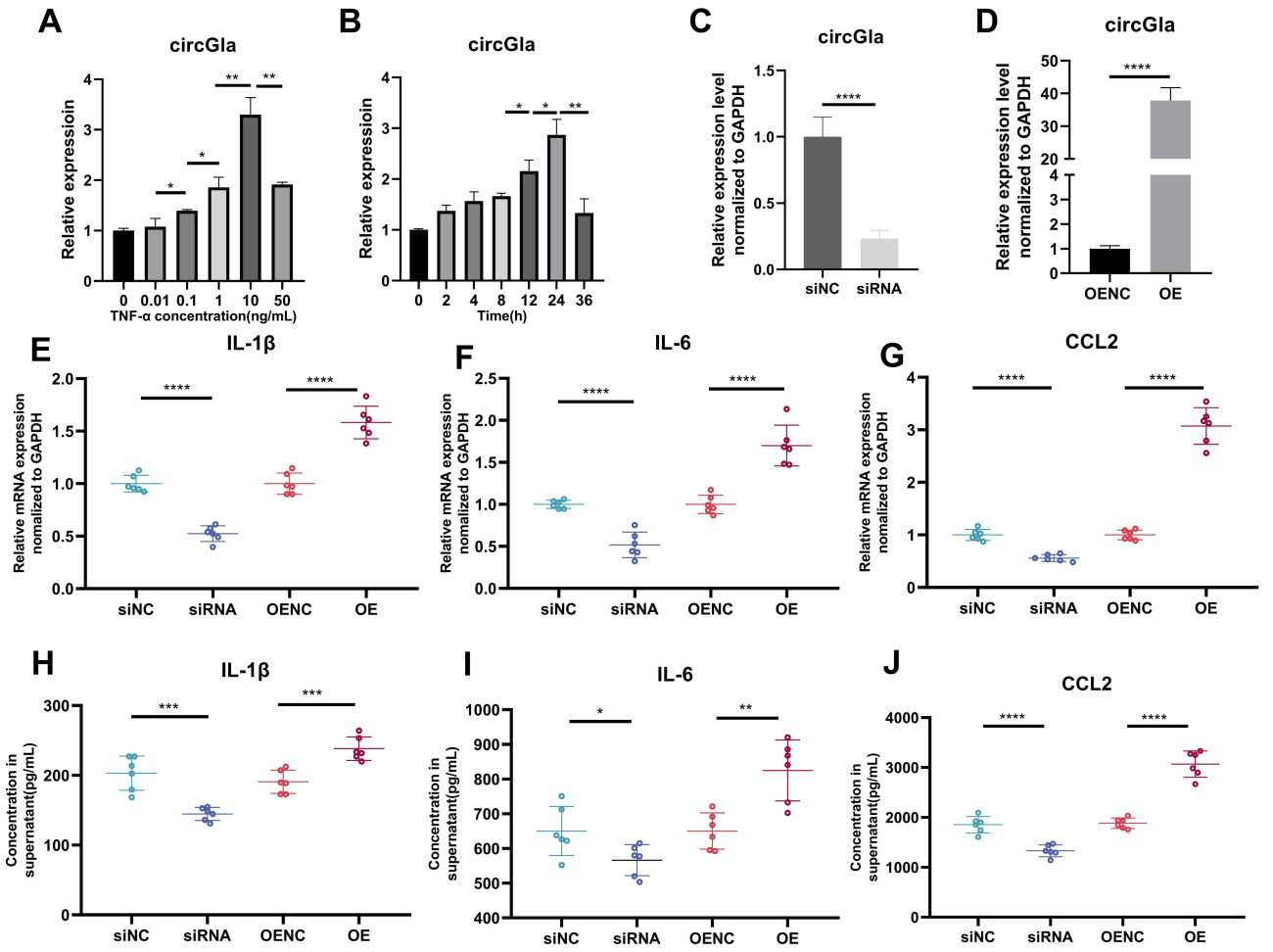

Figure 3 Astrocyte inflammatory mediator changes due to circGla. (**A** and **B**) The circGla mRNA level changes over time (0, 2, 4, 8, 12, 24, and 36 h) after 10 ng/mL TNF-α stimulation and over concentration gradients (0, 0.01, 0.1, 1, 10, 50 ng/mL), detected by RT-qPCR. At 24 h with 10 ng/mL, the most significant difference was obtained; hence these values were selected for subsequent in vitro experiments. In the next experiments, mouse astrocytes with an appropriate cell density in 6-well plates were first transfected with siRNA/siNC or OE/OENC plasmid and then 10 ng/mL TNF-α stimulation was added for 24 h. (**C** and **D**) After transfection, the mRNA levels of circGla in mouse astrocytes were detected by RT-qPCR to investigate the transfection efficacy. (**E–G**) The mRNA levels of the main inflammatory astrocyte-related mediators (IL-1β, IL-6, CCL2) were detected by RT-qPCR (n = 6). The upregulation of circGla elevated the expression of pro-inflammatory mediators. (**H–J**) ELISA was performed to detect the inflammatory mediators (IL-1β, IL-6, CCL2) in astrocyte culture supernatant (n = 6). ns: no significance; *P < 0.05; **P < 0.01; ***P < 0.001; **** P < 0.0001.

circGla Could Regulate Astrocyte Inflammation by Binding to miR-488

circRNAs often serve as molecular sponges binding to miRNAs with complementary sequences and inhibiting their original functions. Considering the abundant and stable cytoplasmic content of circGla, we examined the ability of circGla to bind to miRNAs, and the possible binding sequence of miRNA miR-488, which previously decreased in the mouse spinal cord after SCI modeling (GSE158194, https://www.ncbi.nlm.nih.gov/gds), was predicted by referring to the TargetScan website (http://www.Targetscan.org) (Figure 4A). The RIP assay was conducted to test the binding of the two molecules. circGla was amplified from the immunoprecipitate, which was pulled down by the AGO2 antibody, indicating the binding of circGla with miRNAs through AGO2 (Figure 4B). In the co-transfected C8D1A cells, the binding of circGla and miR-488 was also confirmed through the dual-luciferase reporter assay (Figure 4C). Therefore, miR-488 was selected for further inflammatory functional experiments. To verify the binding of circGla to miR-488, the relative miR-488 expressions in mouse astrocyte groups with different circGla levels were determined through RT-qPCR (Figure 4D). As shown in Figure 4D, miR-488 expression was upregulated in the circGla siRNA-treated group compared with the siNC group. By contrast, miR-488 expression in the circGla overexpression group exhibited the opposite trend. A similar tendency was also observed in the animal experiments (Figure 4E) where relatively higher miR-488 levels were observed in the spinal cord of the SCI+sh-

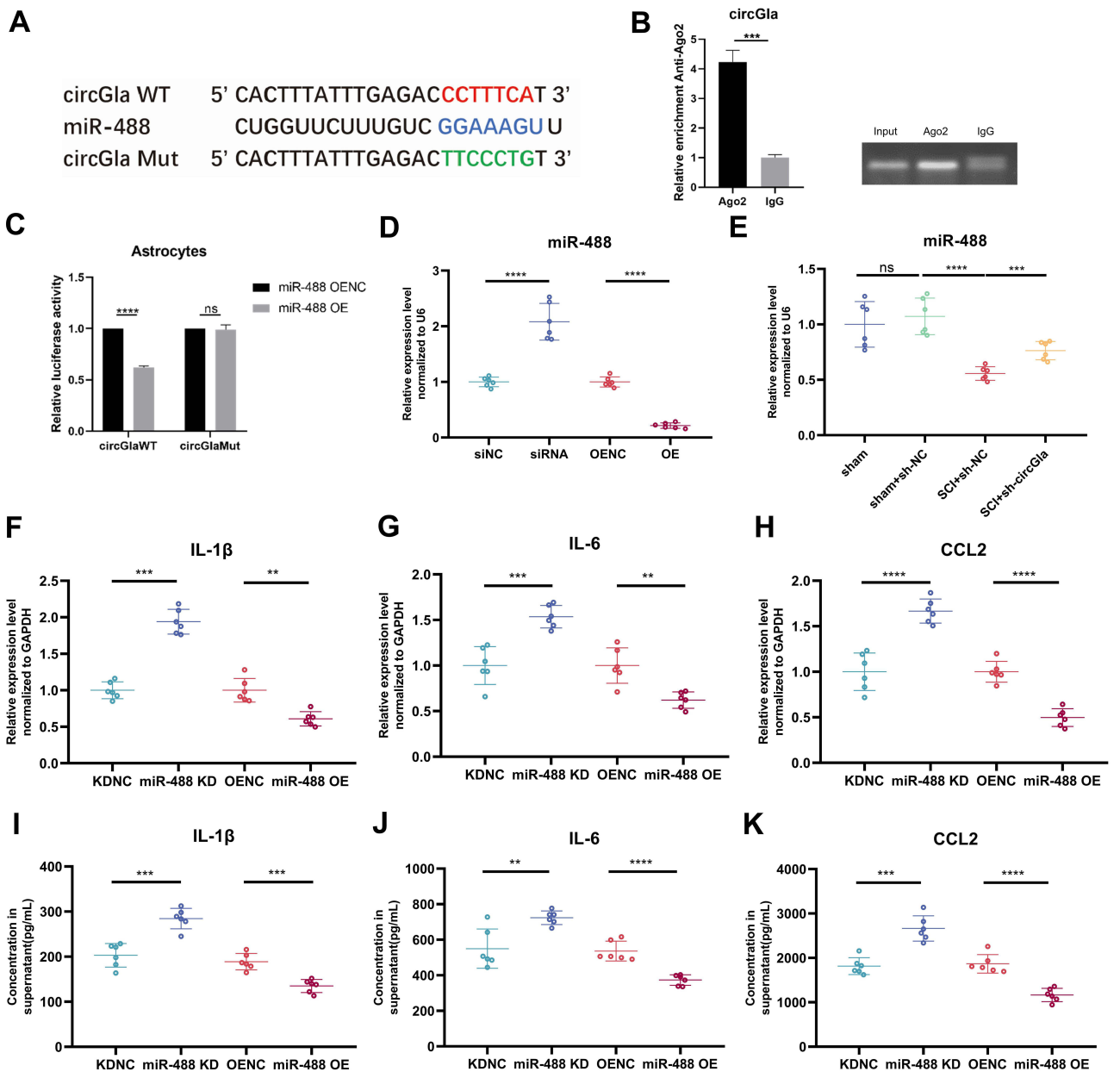

Figure 4 miR-488 as a target of circGla. (**A**) Schematic graph of the binding sites between circGla and miR-488, as predicted by miRanda (http://www.microrna.org) and TargetScan. The target sequence for dual-luciferase reporter assay. (**B**) RIP analysis of the circGla level in the immunoprecipitate of AGO2 antibody from mouse astrocytes. (**C**) Relative luciferase activities with the circGla WT or MUT and miR-488 mimics or mimic NC from dual-luciferase assays. (**D**) The relative miR-488 levels in astrocytes transfected with siRNA/siNC or OE/OENC plasmids to circGla, as detected by RT-qPCR (n = 6). U6 served as an internal reference. (**E**) RT-qPCR revealed a reversed miR-488 level in the mouse model infected with sh-circGla AAV (n = 6). (**F–H**) The RT-qPCR results of the relative mRNA expressions for the main inflammatory astrocyte-related mediators (IL-1β, IL-6, CCL2) in astrocytes transfected with miR-488 inhibitor NC or miR-488 inhibitors and miR-488 mimic NC or miR-488 mimics, after 10 ng/mL TNF-α stimulation (n = 6). (**I–K**) ELISA for the protein levels of the main inflammatory astrocyte-related mediators (IL-1β, IL-6, CCL2) in the supernatant of the astrocytes transfected with miR-488 inhibitor NC or miR-488 inhibitors, miR-488 mimic NC or miR-488 mimics, after 10 ng/mL TNF-α stimulation (n = 6). ns: no significance; **P < 0.01; ***P < 0.001; ****P < 0.0001.

circGla group mice compared with those of the SCI+sh-NC group mice. The aforementioned in vivo and in vitro results proved that circGla targets miR-488 and regulates the miR-488 content in the mouse astrocytes and spinal cord in the inflammatory state. We then explored the miR-488 function in the mouse astrocytes under the inflammatory condition. To achieve the effect of downregulating or upregulating miR-488 expressions, the miR-488 inhibitors or mimics were transfected into the mouse astrocytes of the corresponding experimental groups. The inhibitor or mimic NC was transfected into the control group cells. After 24 h of stimulation with 10 ng/mL TNF-α, cells in each group were collected for RT-qPCR. The

supernatants from each group were used for the subsequent ELISA. miR-488 downregulation in the TNF-α-stimulated astrocytes increased the mRNA levels of the major astrocyte-related inflammatory cytokines, whereas the increase in the miR-488 content triggered an opposite tendency (Figure 4F–H). The major inflammatory cytokines in the serum exhibited a similar pattern (Figure 4I–K). The aforementioned findings confirmed that the miR-488 content was negatively correlated with the degree of inflammation in the function and that the proinflammatory function of circGla was realized through its binding to miR-488.

MEKK1 Was Found to Be a Target for circGla/miR-488

The aforementioned studies demonstrated the function of the downstream molecule of circGla, that is, miR-488, in astrocyte inflammation. Based on the typical pattern of the circRNA action, we continued to search for the downstream target molecule. In a previous study, MEKK1 was found to bind to miR-488 in HEK-293T cells.[22] Wild-type and mutant sequences in the MEKK1 3′-UTR binding site (to miR-488), as previously reported, were used for firefly and hydronephrosis luciferase plasmid construction. The relative fluorescence intensity revealed that the miR-488 mimics failed to bind to the mutant plasmid product (Figure 5A), thereby validating the correspondence between miR-488 and MEKK1 in astrocytes. RNA and protein levels unveiled that higher miR-488 levels corresponded to lower MEKK1 mRNA and protein levels (Figure 5B–I). Moreover, lower miR-488 levels corresponded to higher MEKK1 levels. Furthermore, higher circGla levels in the astrocytes corresponded to higher MEKK1 mRNA and protein levels, and vice versa (Figure 5C–K). MEKK1 plays a role in the activation of the JNK/p38 MAPK pathway.[22,23] Our results suggested that the relative levels of the phosphorylated proteins p-JNK and p-p38 increased with a decrease in miR-488 levels, and vice versa (Figure 5D–I). Meanwhile, p-JNK and p-p38 levels were reduced in the circGlasiRNA-treated astrocytes compared with siNC-transfected astrocytes, whereas transfection with the overexpression plasmid of circGla increased the levels of the aforementioned two proteins (Figure 5F–K). To verify whether circGla regulated MEKK1 through miR-488 in the mouse astrocytes, circGla and miR-488 levels were simultaneously regulated in the same astrocytes, and MEKK1 protein levels were then examined. miR-488 inhibition resulted in higher MEKK1 levels in the circGla siRNA-transfected astrocytes in the inflammatory state (Figure 5L–M). By contrast, in the circGla overexpression plasmid-transfected astrocytes, transfection with the reduced MEKK1 levels compared with that with the NC plasmid (Figure 5N and O). Taken together, these data suggested that MEKK1 is a target of miR-488, a downstream molecule of circGla, in regulating the inflammatory state of astrocytes.

Discussion

Currently, functional neurorestoration is realizable after CNS injury and during neurodegeneration, which includes SCI. Varying neurorestorative treatments have been applied to improve SCI patients' neurological functions and their quality of life.[24] Researchers have been exploring effective treatments for SCIs. The process of secondary damage in SCIs appears to be more manageable than primary injuries. Regulating secondary injuries at a relatively early stage of the process is critical.[25,26] Inflammation, a crucial component of the secondary injury process of SCI, significantly influences the SCI recovery process. Therefore, targeting the inflammation process in secondary injury after SCI is among the recent directions of SCI research.[8,21,27,28]

In inflammation, resident cells are activated in the spinal cord.[10] After receiving external insults, astrocytes, the most widely distributed cells in the CNS, undergo heterogeneous activation from their original resting state, thereby exhibiting different molecular patterns and functions.[11,29] Activated astrocytes participate in complex cellular and molecular interactions in the post-injury inflammatory microenvironment. They are also involved in the primary amplification cascade of inflammation, which then affects the neurological function in terms of damage repair and regeneration.[30] Modulation of astrocytes activated in response to post-SCI inflammation may affect the inflammatory state, and subsequently the subsequent process of post-SCI neurological recovery, a recovery process exemplified through functional experiments in classical animal models of SCI.

We here conducted cell and animal experiments to demonstrate the role of circGla in post-SCI astrocytes. A mechanically precise percussion apparatus was used for modeling, and circGla expression was found to be significantly upregulated in 3-day tissues after SCI, as demonstrated by previous sequencing results. The reverse splicing

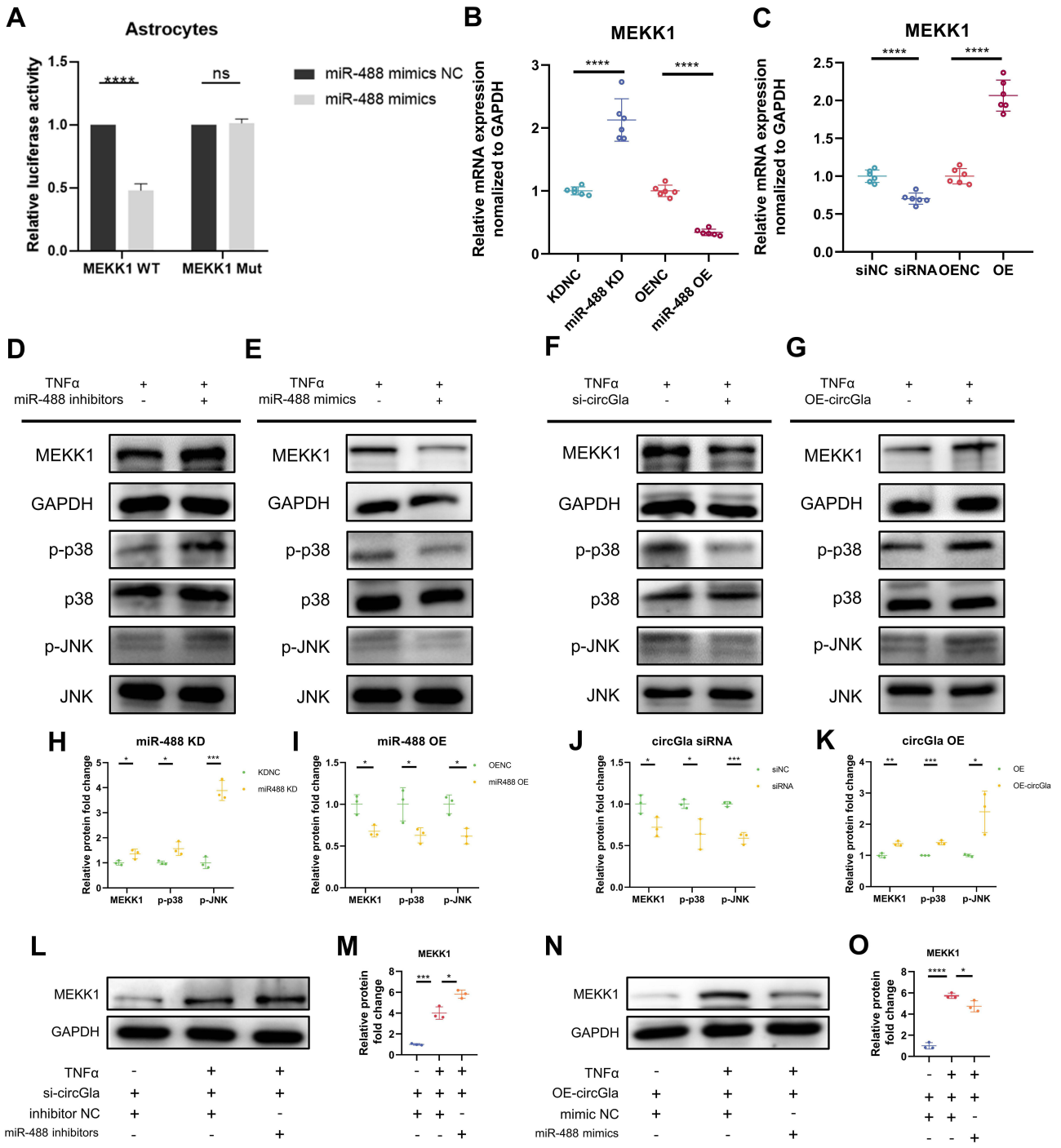

Figure 5 Correlation experiments for circGla/miR-488/MEKK1. (**A**) Dual-luciferase reporter assays revealed the relative luciferase activity produced by the MEKK1 WT or MUT and miR-488 mimics, mimic NC transfection. (**B**) The mRNA levels of MEKK1 in mouse astrocytes transfected with miR-488 inhibitor NC or miR-488 inhibitors and miR-488 mimic NC or miR-488 mimics after 10 ng/mL TNF-α stimulation (n = 6). (**C**) The mRNA levels of MEKK1 in mouse astrocytes transfected with siRNA/siNC or OE/OENC plasmids to circGla after 10 ng/mL TNF-α stimulation, as detected by RT-qPCR (n = 6). (**D** and **E**) The relative protein expression of MEKK1, phosphorylated-p38, p38, phosphorylated-JNK, JNK protein, in astrocytes transfected with miR-488 inhibitor NC or miR-488 inhibitors, miR-488 mimic NC or miR-488 mimics, and 10 ng/mL TNF-α stimulation (n = 3), as determined by Western blotting. (**F** and **G**) Representative images of the relative protein expression of MEKK1, phosphorylated-p38, p38, phosphorylated-JNK, JNK protein, in astrocytes transfected with siRNA/siNC or OE/OENC plasmids to circGla, and 10 ng/mL TNF-α stimulation, as determined by Western blotting. (**H-K**) **H, I, J,** and **K** panels represent the quantitative results for the Western blotting assay in **D, E, F,** and **G,** respectively, as analyzed by the Image J software. n = 3. (**L** and **M**) Representative Western blotting images for the MEKK1 expression in mouse astrocytes with circGla single knockdown or joint knockdown with miR-488 (**L**) and its quantitative image (**M**). n = 3. (**N** and **O**) Representative Western blotting images for the MEKK1 expression in mouse astrocytes with a circGla single overexpression or the joint expression with miR-488 (**N**) and its quantitative image (**O**), n = 3. ns: no significance; *P < 0.05; **P < 0.01; ***P < 0.001; ****P < 0.0001.

pattern and circular structure of circGla were also validated through molecular experiments. Subsequent experiments displayed its localization in the astrocytic cytoplasm.

To investigate whether circGla, whose content was differentially altered before and after SCI, has no function in animals, the circGla content was knocked down in the spinal cord of the 5-week-old female C57BL6 mice. Viruses and astrocytes were found to be co-localized in the spinal cord tissue, and the effect of the viral knockdown was validated. Subsequently, the mice were randomized into four groups (sham group, sham+sh-NC group, SCI+sh-NC group, and SCI +sh-circGla group), and their long-term functional recovery was assessed. Mice in the circGla downregulated group had higher functional scores and better performance in the open-field test, which suggested that lower circGla content is associated with higher post-SCI recovery. However, the virus we used was not originally designed to target astrocytes, which somewhat affects the specificity of the results. Additionally, the off-target effects of AAV viruses are worth noting. Compared with previous studies, we complemented and enriched functional exploration approaches.

The short-term pathological process following SCI strongly affects long-term recovery. To investigate whether circGla achieves its effect on functional recovery by affecting post-SCI early inflammation, we focused on the inflammatory manifestation of the mouse spinal cord 3 days after SCI, the same time point as sequencing. A relatively lower inflammatory MRI manifestation was noted in the circGla knockdown group mice at 3 dpi. The relatively low inflammatory state in the SCI+sh-circGla group was further verified on the basis of levels of major inflammatory factors in the spinal cord tissue and serum, suggesting that circGla has pro-inflammatory functions. Our in vivo results suggest that lower circGla levels correlate with reduced inflammatory status and improved performance in behavioral tests. These findings support that circGla may exert neurotoxic effects by promoting inflammation post-injury, resulting in reduced neurofunctional recovery.

Using mouse astrocytes, we continued to explore the proinflammatory function and possible mechanisms of circGlain vitro. The post-SCI inflammatory environment to which in vivo astrocytes are exposed was mimicked. The expression of inflammatory cytokines was elevated or decreased in the astrocytes with upregulated or downregulated circGla following TNF-α stimulation, suggesting that circGla has a similar proinflammatory effect on astrocytes in vitro. In in vivo experiments, we knocked down the expression of circGla in the spinal cord of mice. The knockdown group showed lower levels of TNFα, IL-1β, IL-6 expression after injury, and demonstrated relatively better behavioral recovery performance. In the mouse astrocyte line C8D1A, knocking down circGla also resulted in reduced levels of classic inflammatory factors IL-1β, IL-6, and CCL2 in astrocytes under inflammatory stimulation in the knockdown group, consistent with findings in vivo.

According to our previous sequencing results, miR-488 differed significantly before and after SCI and exhibited an inflammation-related function in astrocytes.[22,31] Based on the sites predicted to bind to circGla, we confirmed the binding molecule. In miR-488-knocked down or overexpressed astrocytes, we demonstrated that miR-488 functions as an inflammatory regulator. High miR-488 levels may correlate with a low astrocytic inflammatory state.

Our previous group found that miR-488 binds to MEKK1 in HEK293T cells, and circPrkcsh functions through miR-488/MEKK1 in microglia.[22] Our results also showed the binding of miR-488 with MEKK1 in mouse astrocytes. Upregulation or knockdown of circGla or miR-488 alone in the astrocytes affected MEKK1 mRNA and protein levels, respectively. The MEKK1 protein content was modulated for circGla and miR-488, miR-488 and MEKK1 intermolecular correlations. When circGla and miR-488 were both regulated in the astrocytes, the MEKK1 protein contents demonstrated that circGla, miR-488, and MEKK1 are correlated. The MEKK1 protein exhibited a wide range of biological activities. Being a crucial node upstream of the JNK/p38 MAPK signaling pathway, MEKK1 profoundly affects downstream inflammatory pathways. Western blotting exhibited altered p-p38 and p-JNK protein levels parallel with the trend of MEKK1 protein changes in different astrocyte treatment groups. This finding could also explain the aforementioned changes in inflammatory factors.[32,33]

However, our current study still has limitations. First, astrocytes were stimulated with TNF-α to mimic the inflammatory state of post-SCI astrocytes, which could not fully mimic the complicated inflammatory state that astrocytes experience in vivo after the injury. Second, circGla was only studied in astrocytes, and its role in microglia and neuron may subsequently be explored. Human spinal cord tissue accessibility is inherently limited due to ethical and practical constraints. Consequently, only results from cell and animal experiments are included in our current study,

which to some extent limits the significance of our study. Finally, other pathways may be responsible for the action of circGla, which needs to be investigated in our subsequent studies. circGla may also act via other pathways; and, this needs to be investigated through subsequent studies.

While the primary focus of this study has been on astrocytes, we acknowledge the importance of a broader cellular landscape in SCI. In particular, microglia, as another essential glial cell type, play a pivotal role in initiating and modulating the inflammatory response following SCI. Its main functions are migration to the site of injury, regulation of inflammatory response, and clearance of cellular debris. Their activation not only contributes to the repair of neural tissue, but may also trigger excessive inflammation, which has a dual impact on the recovery process.[7,34,35] Whether circGla plays a role in microglia is one of our next research directions, which will help us have a more comprehensive understanding of the ways circGla plays a role in spinal cord injury.In the future, we will continue to actively seek the clinical translation of key molecules found in animal experiments, such as starting from their homology with human derived molecules.

Conclusion

In conclusion, we found that circGla can affect the inflammatory state and long-term functional recovery after SCI by regulating miR-488/MEKK1 in mouse astrocytes. This finding is potentially valuable for SCI treatment in the future.

Abbreviations

circRNA, circular RNA; miRNA, microRNA; dpi, day(s) post injury; Gla, galactosidase alpha gene; SCI, spinal cord injury; HE staining, Hematoxylin-eosin staining; SCI 3d, 3 days after spinal cord injury model establishment; GAPDH, glyceraldehyde-3-phosphate dehydrogenase; RT-qPCR, quantitative reverse transcription polymerase chain reaction; DAPI,4',6-diamidino-2-phenylindole; cDNA, complementary DNA; gDNA, genome DNA; FISH, fluorescence in situ hybridization; 18S rRNA, 18S ribosomal RNA; GFAP, glial fibrillary acidic protein; GFP, green fluorescent protein; PBS, phosphate buffered saline; sh-circGla AAV, pAAV-U6-shcircGla-CMV-EGFP-WPRE; BMS scoring, Basso Mouse Scale scoring; MRI, magnetic resonance imaging; ELISA, Enzyme-linked immunosorbent assay; TNF-α, tumor necrosis factor-α; siRNA/siNC, small interfering RNA targeting at circGla/ negative control small interfering RNA; OE/OENC, overexpression/ negative control; RIP, RNA immunoprecipitation; AGO2, Argonaute-2; WT, wild type sequence for circGla expression plasmid; MUT, mutant sequence for circGla expression plasmid; U6, small nuclear RNA U6; NC, negative control; MEKK1, mitogen-activated protein kinase kinasekinase 1; JNK, c-Jun N-terminal kinase.

Acknowledgments

We thank the support from the following institutions: Research Center of Basic Medicine, Research Center of Translational Medicine and Laboratory Animal Center of Central Hospital Affiliated to Shandong First Medical University.

The graphic abstract (Shao, Q. (2024) BioRender.com/w80z972) and schematic diagram Figure 2C (Shao, Q. (2024) BioRender.com/o77y647) are produced in Biorender.com.

Funding

The study was supported by the National Natural Science Fund of China [82071383, 82371392], Natural Science Foundation of Shandong Province (Key Project) [ZR2020KH007], the "Taishan Scholar Distinguished Expert Program" of Shandong Province [tstp20231257], Natural Science Foundation of Shandong Province (ZR2022QC222), Youth Science Foundation of Shandong First Medical University (202201-132) and Jinan Municipal Health Commission Science and Technology Plan Project (2023-1-2; 2023-1-8; 2024102001; 2024202003).

Disclosure

The authors report no conflicts of interest in this work.

References

1. Rubiano AM, Carney N, Chesnut R, Puyana JC. Global neurotrauma research challenges and opportunities. *Nature*. 2015;527(7578):S193–S197. doi:10.1038/nature16035
2. Chen C, Qiao X, Liu W, Fekete C, Reinhardt JD. Epidemiology of spinal cord injury in China: a systematic review of the Chinese and English literature. *Spinal Cord*. 2022;60(12):1050–1061. doi:10.1038/s41393-022-00826-6
3. Jazayeri SB, Kankam SB, Golestani A, et al. A systematic review and meta-analysis of the global epidemiology of pediatric traumatic spinal cord injuries. *Eur J Pediatr*. 2023;182(12):5245–5257. doi:10.1007/s00431-023-05185-9
4. Zhou H, Lou Y, Chen L, et al. Epidemiological and clinical features, treatment status, and economic burden of traumatic spinal cord injury in China: a hospital-based retrospective study. *Neural Regen Res*. 2024;19(5):1126–1133. doi:10.4103/1673-5374.382257
5. Khorasanizadeh M, Yousefifard M, Eskian M, et al. Neurological recovery following traumatic spinal cord injury: a systematic review and meta-analysis. *J Neurosurg Spine*. 2019;30:683–699. doi:10.3171/2018.10.SPINE18802
6. Lima R, Monteiro A, Salgado AJ, Monteiro S, Silva NA. Pathophysiology and Therapeutic Approaches for Spinal Cord Injury. *Int J Mol Sci*. 2022;23(22).
7. Hellenbrand DJ, Quinn CM, Piper ZJ, Morehouse CN, Fixel JA, Hanna AS. Inflammation after spinal cord injury: a review of the critical timeline of signaling cues and cellular infiltration. *J Neuroinflammation*. 2021;18(1):284. doi:10.1186/s12974-021-02337-2
8. Jin Y, Song Y, Lin J, et al. Role of inflammation in neurological damage and regeneration following spinal cord injury and its therapeutic implications. *Burns Trauma*. 2023;11:tkac054. doi:10.1093/burnst/tkac054
9. Hart CG, Karimi-Abdolrezaee S. Recent insights on astrocyte mechanisms in CNS homeostasis, pathology, and repair. *J Neurosci Res*. 2021;99(10):2427–2462. doi:10.1002/jnr.24922
10. Lukacova N, Kisucka A, Kiss Bimbova K, et al. Glial-Neuronal Interactions in Pathogenesis and Treatment of Spinal Cord Injury. *Int J Mol Sci*. 2021;22(24):13577. doi:10.3390/ijms222413577
11. Boghdadi AG, Teo L, Bourne JA. The Neuroprotective Role of Reactive Astrocytes after Central Nervous System Injury. *J Neurotrauma*. 2020;37(5):681–691. doi:10.1089/neu.2019.6938
12. Bao H, Li J, Zhao Q, Yang Q, Xu Y. Circular RNAs in Breast Cancer: an Update. *Biomolecules*. 2024;14(2):158. doi:10.3390/biom14020158
13. Chen M, Lai X, Wang X, et al. Long Non-coding RNAs and Circular RNAs: insights Into Microglia and Astrocyte Mediated Neurological Diseases. *Front Mol Neurosci*. 2021;14:745066. doi:10.3389/fnmol.2021.745066
14. Nemeth K, Bayraktar R, Ferracin M, Calin GA. Non-coding RNAs in disease: from mechanisms to therapeutics. *Nat Rev Genet*. 2024;25(3):211–232. doi:10.1038/s41576-023-00662-1
15. Sun Y, Chu S, Wang R, et al. Non-coding RNAs modulate pyroptosis in myocardial ischemia-reperfusion injury: a comprehensive review. *Int J Biol Macromol*. 2024;257(Pt 1):128558. doi:10.1016/j.ijbiomac.2023.128558
16. Zhu J, Huang F, Hu Y, et al. Non-Coding RNAs Regulate Spinal Cord Injury-Related Neuropathic Pain via Neuroinflammation. *J Inflamm Res*. 2023;16:2477–2489. doi:10.2147/JIR.S413264
17. Najafi S, Aghaei Zarch SM, Majidpoor J, et al. Recent insights into the roles of circular RNAs in human brain development and neurologic diseases. *Int J Biol Macromol*. 2023;225:1038–1048. doi:10.1016/j.ijbiomac.2022.11.166
18. Yang L, Wilusz JE, Chen -L-L. Biogenesis and Regulatory Roles of Circular RNAs. *Annu Rev Cell Dev Biol*. 2022;38:263–289. doi:10.1146/annurev-cellbio-120420-125117
19. Sanger HL, Klotz G, Riesner D, Gross HJ, Kleinschmidt AK. Viroids are single-stranded covalently closed circular RNA molecules existing as highly base-paired rod-like structures. *Proc Natl Acad Sci U S A*. 1976;73(11):3852–3856. doi:10.1073/pnas.73.11.3852
20. Basso DM, Fisher LC, Anderson AJ, Jakeman LB, McTigue DM, Popovich PG. Basso Mouse Scale for locomotion detects differences in recovery after spinal cord injury in five common mouse strains. *J Neurotrauma*. 2006;23(5):635–659. doi:10.1089/neu.2006.23.635
21. Freyermuth-Trujillo X, Segura-Uribe JJ, Salgado-Ceballos H, Orozco-Barrios CE, Coyoy-Salgado A. Inflammation: a Target for Treatment in Spinal Cord Injury. *Cells*. 2022;11(17):2692. doi:10.3390/cells11172692
22. Li X, Kang J, Lv H, et al. CircPrkcsh, a circular RNA, contributes to the polarization of microglia towards the M1 phenotype induced by spinal cord injury and acts via the JNK/p38 MAPK pathway. *FASEB J*. 2021;35(12):e22014. doi:10.1096/fj.202100993R
23. Chang L, Karin M. Mammalian MAP kinase signalling cascades. *Nature*. 2001;410(6824):37–40. doi:10.1038/35065000
24. Huang H, Sanberg PR, Chen L, Chopp M, Sharma HS. Explanation and elaboration: development of Beijing Declaration of International Association of Neurorestoratology. *J Neurorestoratology*. 2023;11(2):100057. doi:10.1016/j.jnrt.2023.100057
25. Yin Z, Wan B, Gong G, et al. ROS: executioner of regulating cell death in spinal cord injury. *Front Immunol*. 2024;15:1330678. doi:10.3389/fimmu.2024.1330678
26. Hu X, Xu W, Ren Y, et al. Spinal cord injury: molecular mechanisms and therapeutic interventions. *Signal Transduct Target Ther*. 2023;8(1):245. doi:10.1038/s41392-023-01477-6
27. Dokalis N, Prinz M. Resolution of neuroinflammation: mechanisms and potential therapeutic option. *Semin Immunopathol*. 2019;41(6):699–709. doi:10.1007/s00281-019-00764-1
28. Sterner RC, Sterner RM. Immune response following traumatic spinal cord injury: pathophysiology and therapies. *Front Immunol*. 2022;13:1084101. doi:10.3389/fimmu.2022.1084101
29. Wang J, Cheng C, Liu Z, et al. Inhibition of A1 Astrocytes and Activation of A2 Astrocytes for the Treatment of Spinal Cord Injury. *Neurochem Res*. 2023;48(3):767–780. doi:10.1007/s11064-022-03820-9
30. Reid JK, Kuipers HF. She Doesn't Even Go Here: the Role of Inflammatory Astrocytes in CNS Disorders. *Front Cell Neurosci*. 2021;15:704884. doi:10.3389/fncel.2021.704884
31. Chen J-N, Zhang Y-N, Tian L-G, Zhang Y, X-Y L, Ning B. Down-regulating Circular RNA Prkcsh suppresses the inflammatory response after spinal cord injury. *Neural Regen Res*. 2022;17(1):144–151. doi:10.4103/1673-5374.314114
32. Ding Y, Chen Q. The NF-κB Pathway: a Focus on Inflammatory Responses in Spinal Cord Injury. *Mol Neurobiol*. 2023;60(9):5292–5308. doi:10.1007/s12035-023-03411-x
33. Kasuya Y, Umezawa H, Hatano M. Stress-Activated Protein Kinases in Spinal Cord Injury: focus on Roles of p38. *Int J Mol Sci*. 2018;19(3). doi:10.3390/ijms19030867

34. Xu L, Wang J, Ding Y, Wang L, Zhu Y-J. Current Knowledge of Microglia in Traumatic Spinal Cord Injury. *Front Neurol*. 2021;12:796704. doi:10.3389/fneur.2021.796704
35. Orr MB, Gensel JC. Spinal Cord Injury Scarring and Inflammation: therapies Targeting Glial and Inflammatory Responses. *Neurotherapeutics*. 2018;15(3):541–553. doi:10.1007/s13311-018-0631-6